a point-by-point response to the reviews

Response to referee #1's comments

The author would like to thank Anonymous referee #1 for the constructive and helpful suggestions on this manuscript.
We replied to 1 general comment and 8 specific comments.

General Comment

C1. The paper applies a linearization of the ISRF for the retrieval of ozone profiles from OMI measurements. The linearization approach was introduced by Beirle et al., 2017 (BE17 hereafter), which is referenced appropriately. However, the authors should generally specify more clearly which steps are adopted from BE17, and what are original/new ideas/methods/results of their study. The adaptation of the ISRF parameterization for radiances seems to be new and interesting. However, there are some complications which have to be investigated in detail and discussed thoroughly. I recommend publication in AMT after these major revisions have been made.

R1. According to this comment, we have specified what this paper adopted from BE17 and what we advanced in implementing the slit function linearization in Section 2.2, as following " In Beirle et al. (2017) a slit function linearization was implemented only to fit solar irradiances from GOME-2. We implement the slit function linearization to fit radiances in the SAO ozone profile algorithm (Liu et al. 2010), (Liu et al. 2010). ~ In DOAS analysis, the pseudo absorber is defined as $\frac{\partial S}{\partial p} \otimes \sigma_h$ (σ_h is a high-resolution absorption cross section), which could be calculated at a computationally low-cost. In our optimal estimation based ozone profile retrievals, it is conceptually defined as $\frac{\partial S}{\partial p} \otimes I_h$ (I_h is a high-resolution simulated radiance), which is computationaly very expensive because of on-line radiative calculation for a ~ 60 nm wide fit window on the spatial pixel-to-pixel basis. We now introduce how to implement the slit function linearization to derive the derivatives of the OMI radiances with respect to slit function changes in two different radiative transfer approaches used in the SAO ozone profile algorithm, i.e., the effective cross section approach in Liu et al (2010) and the updated high-resolution convolution approach described in Kim et al. (2013), respectively."

Specific Comments

C1. Irradiance vs. radiance. BE17 presented the ISRF parameterization for a fit of a measured irradiance to a high-resolution solar atlas. In the current study, the authors apply the parameterization to radiances. This implies that the PAs depend on the Ozone column, and the spectral structures are different for each satellite pixel! This is not clearly stated in the manuscript and should be quantified (i.e. compare the PAs for high/medium/low ozone). Other absorbers have the same effect, i.e. the spectral patterns of the PAs depend e.g. on the strength of the Ring effect (thus on clouds!). This has to be discussed.

R1. - Yes, PAs vary with each satellite pixel. We plotted PAs with respect to slit width for 138 different satellite pixels (S1). The amplitude of PAs increases with latitude/solar zenith angle, but the spectral structures do not change because it arises from errors due to the convolution process of high-resolution absorption cross sections dominated by ozone. This discussion has been included in the revised manuscript, "The amplitude of $\frac{dlnI}{dp}$ varies with different satellite pixels (e.g., ozone profile shape, geometry, and cloud/surface property), but the spectral peak positions do not change because they arise from the errors due to the convolution process of high-resolution absorption cross-sections dominated by ozone." at line 211.

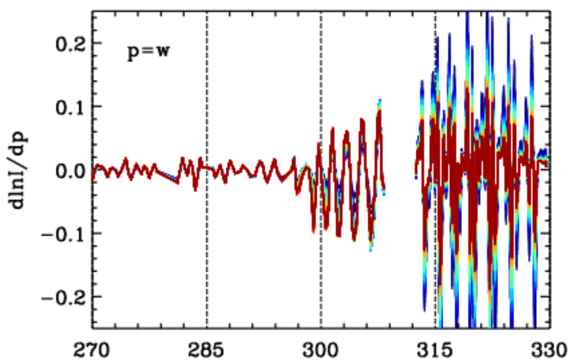

S1. dlnI/dw for 138 pixels at cross-track =15, 0<lat<80, sza<80, and cloud fraction <0.1. The difference colors represent from lower latitudes at red color to higher latitudes at blue color.

- As this review pointed out, other elements of the state vector also have some correlation with cloud fraction, surface albedo, cross track position (e.g. UV1 radiance/ozone cross section shift, UV2 ring scaling parameter, UV1 radiance/irradiance shift). However, it is complex to figure out how these state vectors are interacting with PA coefficients because of weak correlation (<+/- 0.3 for UV1 variables and <+/- 0.1 for UV2 variables) between their jacobians. The PAs are not directly dependent on the strength of the Ring effect in the current implementation, because Ring effect is not fully coupled with the VLIDORT, but calculated using a first-order single scattering model and then scaled with a polynomial to be fitted.

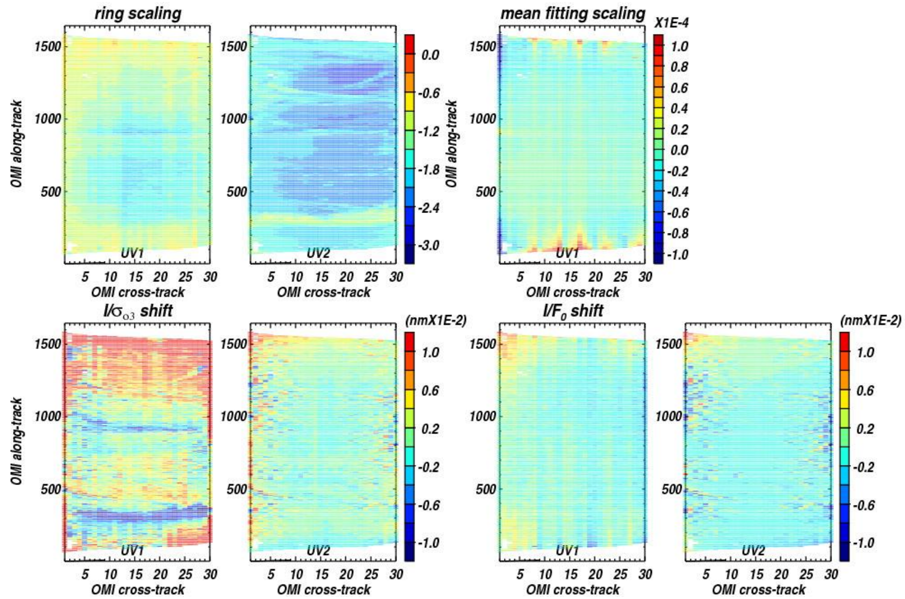

S2. Same as Fig. 4, but for other state vectors.

C2. The abstract contains some statements which are not supported by the presented data:

a) Abstract, first sentence: "reduces the spectral fit residuals caused by the slit function errors". Please add a figure of the spectral analysis with and without PAs in order to substantiate this statement.

b) End of abstract: "Comparisons with ozonesondes demonstrate substantial improvements with the use of PAs". In fig. 10, I see almost no difference, and particularly no "substantial improvements", no matter which function is used nor whether PAs are included or not. Obviously, there are systematic differences remaining compared to Ozone sondes which are not related to the ISRF parameterization.

R2-a. Figs 7 and 8 support the benefit of including a pseudo absorber to improve the fit accuracy. Figure 7 compares the root mean square (RMS) of relative difference (%) between measured and calculated radiances over the UV1 and UV2 ranges, respectively. Including the PAs makes little difference in the UV1 fitting residuals for most of individual pixels (1-5 %), but significantly reduces residuals in the UV2 range (10-25%). In Figure 8, the spectral fit residuals are compared with and without PAs, indicating that including PAs eliminates/reduces some spikes of fitting residuals as well as improves the consistency of the fitting accuracy between using standard and super Gaussians at wavelengths above 300 nm. But as the reduction in the fitting residuals compared to the overall magnitude of the residuals is small, I modify "reduces the spectral fit residuals caused by" to "accounts for"

R2-b. “Substantial” is replaced with “noticeable”. It typically reduces the mean biases with relative to ozonesonde and significantly reduces the standard deviations at high latitudes in the case of super Gaussian. It also makes the mean biases consistent at different latitudes and between the use of standard Gaussian or super Gaussian. In Fig. 10, we think that the benefit of applying ISRF on comparison is not negligible. This figure is re-plotted below in the unit of % and added in the revised manuscript, showing that ~ 5 % of mean biases is eliminated by PA in the lower troposphere. Furthermore, including PAs clearly makes the retrievals consistent between standard and super Gaussians from up to 10% to within 2%.

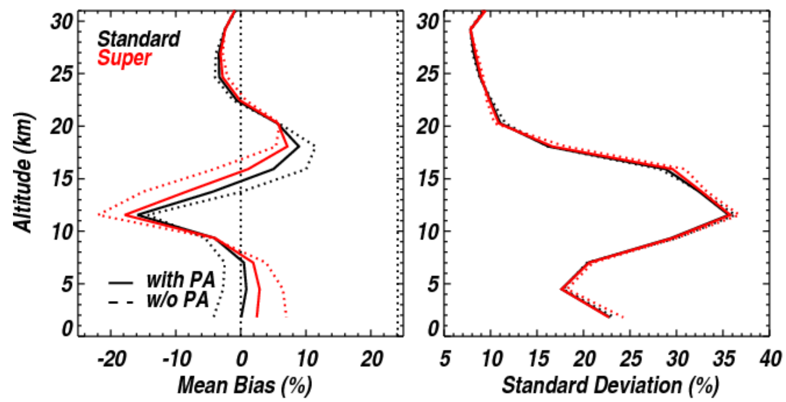

S3. Comparison of relative differences (%) between OMI and ozonesonde as a function of altitude, with different slit function assumption and implementation.

C3. How do the derived ISRFs look like, and how do they compare to the prelaunch measurements performed for OMI?

R3. The comparisons between pre-flight ISRF measurements and the derived ISRFs from solar irradiances are detailed in Sun et al. (2017). In Sun et al. (2017) and this study, the ISRFs are parameterized as a super Gaussian or standard Gaussian from solar irradiance measurements, which are used to convolve high-resolution cross-section spectra into OMI spectral resolution for radiative transfer calculation. In this study, we furthermore focused on implementing the slit function linearization to account for the spectral structures caused by the ISRF difference between radiance and irradiance. A fitting parameter is included as a state vector to adjust the amplitude of this spectral structure with each different pixel. This parameter is named by “pseudo absorber coefficient”, which physically represents not directly ISRFs, but the deviation of ISRFs in radiances from those in solar measurements. ISRFs deviates temporally and spatially and thereby it is complex to represent the ISRFs in radiances.

C4. Fig. 5: What is the meaning of the sum of PAs? Each PA has to be scaled by the respective Delta p. Thus the spectral patterns must not just be added!?

R4. The sum of PAs indicates the total spectral structures caused by the slit function errors. Yes, the PAs cannot be just added together; they will be scaled by the PA coefficients before added together. To avoid the confusion, we have declared it as "the sum of PAs multiplied by corresponding PA coefficients".

- (Caption in Fig.5) Figure 5. (a.1) Pseudo absorber spectra multiplied by corresponding zero order coefficients, $\frac{\partial lnI}{\partial p} \times \Delta p_o$ and (a.2) the sum of them for (left) super Gaussian and (right) standard Gaussian function parameterizations, respectively.
- (Line 250) In the UV1 range, the sum of PAs multiplied by corresponding coefficients, regardless of which Gaussian is assumed as slit function, is very similar because the spectral structure caused by the slit width change is dominant

C5. Fig. 5: The 1st order spectra look wrong. According to Eq. 9, they are 0 in the center of the wavelength window and increase towards the edges (compare Fig. 10 in BE17). The presented spectra look the other way round.

R5. The presented spectra for the zero and first order polynomial coefficients are defined as $\frac{\partial lnI}{\partial p} \times \Delta p_0$ and $\frac{\partial lnI}{\partial p} \times \Delta p_1(\lambda - \bar{\lambda})$). The spectral features by multiplying $(\lambda - \bar{\lambda})$ in PAs are not clearly distinguished in the presented spectra due to the scaling by Δp. It is clearly shown if Δp is taken out as shown in **S4**.

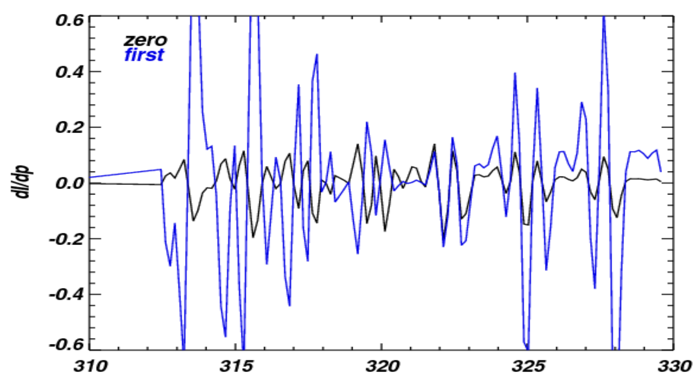

S4. Comparison of PAs for zero and first order polynomial fit.

C6. Fig. 9: Specify the time range of the presented data.

R6. The time range of the resented data has been specified in the corresponding caption and moreover this figure has been changed to Table 1, according to the reviewer 2's comment.

C7. Fig. 10: The unit on the x axis must be DU per km or per vertical layer. Please specify.

R7. The ozone in the unit of DU represent the vertically integrated column for the given altitude range (i.e., DU at each vertical layer) and hence the unit on the x axis should be DU.

C8. Fig. 10: Abbreviation "MB" is not defined.

R8. In the revised manuscript, “MB” and “SD” have been spelled out to Mean Bias and Standard Deviation in the x axis title.

Response to referee #2’s comments

The author would like to thank Anonymous referee #2 for the constructive and helpful suggestions on this manuscript. We replied to 3 major comments and 11 technical comments.

General Comments

This paper is well organized to describe a methodology for reducing the spectral fit residuals. The subject of the paper is appropriate to AMT. Below are a few comments concerning clarifications / extensions for consideration in the final publication in AMT.

Major comments

C1. The PROFOZ algorithm applies the pre-estimated, pixel dependent “soft calibration” factors to the normalized radiances, while conducting the ozone profile retrievals. The “soft calibration” factors seem, by design, accounting for the imperfectness of OMI L1B earthshine radiances and solar irradiances calibration, parameterization of the pixel & wavelength dependent ISRFs, and forward model parameters (absorption cross-sections, surface albedo) etc. The PROFOZ also fits scaling factors for the pre-estimated mean spectral fit residuals (Liu 2010 a, b) for UV1 and UV2 bands accordingly, to account for the remaining systematic errors that were not fully removed from “soft calibration” process. This work suggests fit additional ISRF PA coefficients is necessary for OMI ozone profile retrievals. It seems there might some degeneracy among these approaches. The authors should elaborate whether employing pixel & temporal dependent ‘soft calibration’ factors, or fitting the mean spectral residuals could also achieve the goals same to employing the presented PA approach, in terms of reducing the spectral fit residuals. Are the Jacobians of these PA coefficients, orthogonal to the pre-estimated mean fitting residual spectra, or any other Jacobians of parameters in the retrieval vector?

R1. - As this review pointed out, the soft calibration could partly take into account the remaining systematic errors including the spectral structures due to slit function errors, but it should be taken as a last resort after the known physically treatable errors are considered separately. The applied soft spectra were derived from clear-sky tropical measurements in July 2006 and then applied to everywhere and every day. However, the PAs are calculated at each satellite pixel based on the physics associated with slit convolution proposed in Berlie et al. (2017), and iteratively adjusted with the retrieved coefficients. Therefore, the presented PA approach works much better than soft calibration to reduce the fitting residuals and retrieval errors caused by slit function errors.

- Several peaks of soft spectrum are matched with those of PA jacobians, but the soft spectrum is uncorrelated with PAs (with correlation less than 0.1 in UV1 and 0.3 in UV2) because of other dominant factors causing much higher spectral residuals in the soft spectrum (S1). In addition, PA spectra show a weak correlation with other Jacobians within 0.3 for UV1 variables, but for within 0.1 for UV2 variables (S2). In the revised manuscript, this discussion has been added such as "It should be noted that these spectral structures are weakly correlated with the partial derivatives of radiances with respect to other state vectors (ozone, BrO, cloud fraction, surface albedo, radiance/irradiance shift, radiance/ozone cross section shift, Ring/mean fitting residual scaling factor) within ± 0.3 and ± 0.1 in the UV 1 and UV 2, respectively."

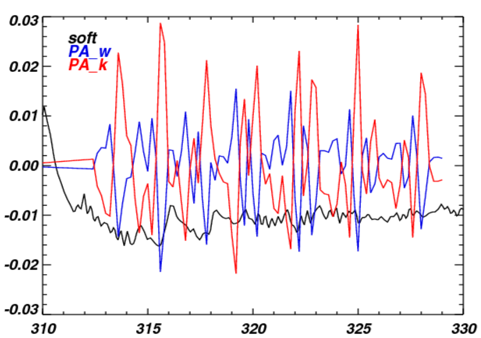

S1. Comparison of soft spectrum with PA jacobians with respect to $\Delta \boldsymbol{w}$ and $\Delta \boldsymbol{k}$, respectively.

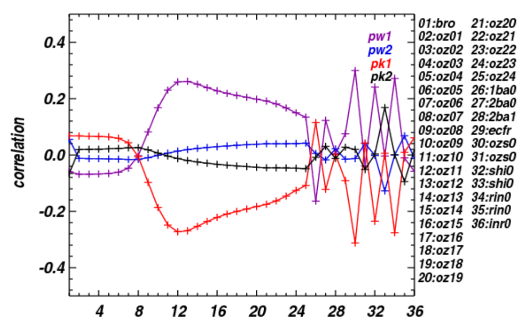

S2. Correlation of jacobians from the other fitting parameters with PA jacobians with respect to $\Delta \boldsymbol{w}$ and $\Delta \boldsymbol{k}$ for UV1 and UV2, respectively.

C2. The authors should obtain time series of retrieved ISRF PA coefficients. Do they show trends similar to Figure 1? At least for Nadir pixel, if not all pixels.

R2. Fig. 1 show the time series of slit function parameters derived from solar irradiance measurements. While the PA coefficients show the deviation from those in Figure 1, so they are not expected to show similar trends as shown in S3. In addition, the PA coefficients can vary from spatial to spatial pixel, and vary along the track for the nadir pixel, so it is not as straightforward to obtain the time series. However, this time series also show the larger variation later in OMI mission, especially in the UV1 due to radiometric calibration issues.

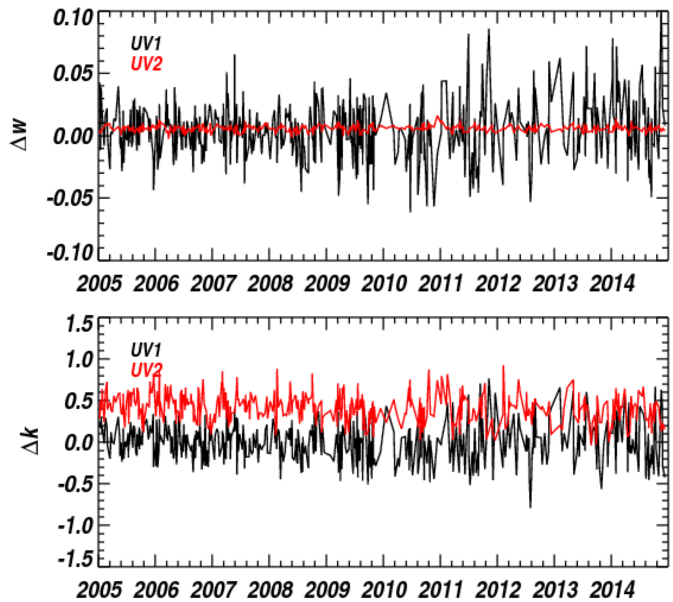

S3. Time-series of PA coefficients for UV1 and UV2, respectively, spatially collocated to 4.3°E, 50.8°N.

C3. A) The authors evaluated the impacts of with/without retrieving PA coefficients on the bias/RMS between retrieved ozone and in-situ ozonesonde measurements (Figure 9). However, the evaluation only made for the period of 2005 to 2008, when OMI instrument was within design lifetime. The authors should also evaluate the performances using the satellite-ozonesonde measurements in other time periods including 2010 and 2012-2013, when the ISRF characteristics were significantly different than the earlier years, as shown in Figure 1. B) The authors should also add some discussions on the possible reasons causing these sharp changes of ISRF characteristics.

R3-a. As well known, there has been concern over the row anomaly effects appearing in 2007 and becoming serious in early 2009, causing trend errors of OMI tropospheric ozone as reported in Huang et al. (2017). Therefore, the period of 2005 to 2008 is focused on the evaluation of including PAs on ozone profile retrievals to avoid any interference with row-anomaly impact. “This evaluation is limited to the period of 2005 through 2008 to avoid interferences with row-anomaly effects appearing in 2007 and becoming serious in early 2009 (Schenkeveld, et al 2017)” has been added in Section 3.2 of the revised manuscript to clarify why the period of 2005 to 2008 is targeted.

R3-b. To explain the sharp changes of ISRF characteristics, "The sharp change and random-noise of these derived slit function parameters might be influenced by the decreasing signal-to-noise ratio (SNR) of solar spectra later in the OMI mission and radiometric errors in solar irradiance due to row anomaly (Sun et al., 2017)." has been added in the revised manuscript.

Technical comments

C1. Have the authors evaluated the impacts of this methodology on the L2 retrieval throughput/yields?

R1. There is no significant impact on throughput. The number of successful retrievals for one orbit measurements is 10880 (standard Gaussian, w/o PA), 10880 (super Gaussian, w/o PA), and 10884 (standard Gaussian, with PA), and 10883 (super Gaussian, with PA)

C2. Line 29, use the statistical numbers on the bias/RMS differences to replace the word "substantial".

R2. The manuscript has been revised to accept this comment as followings.

- (Abstract) "Comparisons with ozonesondes demonstrate noticeable improvements with the use ofwhen using PAs for both standard and super Gaussians, especially for reducing the systematic biases in the tropics and mid-latitudes (mean biases of tropospheric column ozone reduced from -1.4 ~ 0.7 DU to 0.0 ~0.4 DU) and reducing the standard deviations of tropospheric ozone column differences at high-latitudes (by 1 DU for the super Gaussian)."
- (Line 329) "clearly shows that including PAs to account for ISRF differences significantly reduces mean biases below 10 km" ➔ "clearly shows that including PAs to account for ISRF differences significantly reduces mean biases ofby up to ~ 5 % below 10 km"
- (Line 383) "Using super Gaussians, the TCO comparison shows significant improvement in mean biases in mid-latitudes and in standard deviations in high-latitudes. Using standard Gaussians, the TCO comparison also shows significant improvement in mean biases in the tropics" ➔ "In the TCO comparison between OMI and ozonesonde, the mean biases are reduced by 0.2 (0.6) DU and 0.6 (1.4) DU in the tropics (mid-latitude) when super and standard Gaussians are linearized, respectively."

C3. Line 47, the authors should consider to revise "by narrow and weak absorption features of the temperature-dependent Huggins bands (320-360 nm)" to "by the 320-330 nm absorption features residing in the temperature-dependent Huggins bands.", since neither this work nor the referenced studies utilized spectral region > 330 nm in the OMI ozone profile retrievals. "narrow and weak" are general terms and might subjective, e.g., this statement will break down. When comparing within the Chappuis bands, the refereed portion of Huggins bands (>320 nm) is no longer weak.

R3. According to this comment, the indicated sentence has been revised to “by the 310-330 nm absorption features residing in the temperature-dependent Huggins bands”.

C4. Line 50, I will suggest to cite the following studies on OMI ozone profile retrievals, since [1] they made use of the ISRFs from Dirksen et al., [2006] cited a few times in this work, [2] the quality evaluation have been conducted by the comparison with in-situ ozonesonde measurements, [3] same to Liu et al., 2010 cited in this work, these studies were conducted prior to the era of including PA coefficients in the retrieval vector.

R4. We appreciate this suggestion. The suggested references have been cited such as “For space-borne instruments, ISRFs are typically characterized as a function of the detector dimensions using a tunable laser source prior to the launch (Dirksen et al., 2006; Liu et al., 2015; van Hees et al., 2018) and directly used in ozone profile retrievals (e.g., Kroon et al., 2011; Mielonen et al., 2015; Fu et al., 2013; 2018)”

C5. Line 60, might be a typo (radiance repeated twice)?. Do the authors mean “differences in stray light between radiance and irradiance” or “differences in stray light among OMI measurements”?

R5. It is printed-word. It should be “differences in stray light between radiance and irradiance”

C6. Line 61, It seems that “intra-orbit instrumental changes” is duplicating the statement of “the instrument temperature change”. Please clarify (or remove one).

R6. It has been clarified such as “Slit function differences between radiance and irradiance could exist due to scene heterogeneity, differences in stray light between radiance and radiance, and intra-orbit instrumental changes (such as instrument temperature change).”

C7. Figures 1, 2, 4, 5, 7, 8, 9 and 10, increase the tick length for improving their visibility.

R7. All figures have been revised for better visibility.

C8. Figures 5, 6, 8, 9 and 10 captions, state the date/time range of the data presented in the figures. It is not where they are all for 1 July 2006, shown in Figure 4 caption.

R8. In the revised manuscript, all captions include the date/time range of the data.

C9. Figure 9, create a table and move the statistical values to the table. Having all these numbers on the plots resulted in the plots being too busy to read.

R9. The corresponding figure has been changed to Table1.

C10. Figure 10 # please spell out the "MB" and "SD" in the x axis title, - space suffice to hold the full name and they were not defined in the caption. # Add two panels to show the differences among data sets, as a function of altitude?

R10. The a-axis titles have been changed to Mean Bias and Standard Deviation, respectively.

C11. Finally, please keep the 'style' of all figures in a similar fashion. e.g., the panel index of Figure 2 (a), (b) and (c) are inside the plots, while the other figures are outside of the plots. I understand that there is no space for the subtitles outside Figure 2b and 2c, due to the x axis labels. The authors should consider to remove those x axis labels, since all panels could share the one of panel c. Similarly, there are unnecessary axis labels in other figures, e.g., Figures 4, 5, 6, 7, 8, 9, and 10, when some subpanels having an identical scale/range across a row and/or a column, authors should consider remove the unnecessary labels in x or y axis, to help readers easily catch key information presented in the figures.

R11. Thanks for this detailed suggestion. All figures have been revised for better visibility.

a list of all relevant changes

1. All figures have been revised for better visibility.
2. Figure 9 in the older manuscript has been changed to Table 1 in the revised manuscript.

a marked-up manuscript version

Linearization of the effect of slit function changes for improving OMI ozone profile retrievals

Juseon Bak[a,*], Xiong Liu[a], Kang Sun[b], Kelly Chance[a], Jae-Hwan Kim[c]

[a]*Harvard-Smithsonian Center for Astrophysics, Cambridge, MA, USA*

[b]*Research and Education in eNergy, Environment and Water Institute, University at Buffalo, Buffalo, NY, USA*

[c]*Atmospheric Science Department, Pusan National University, Busan, Korea*

*Corresponding Author (juseon.bak@cfa.harvard.edu)

Abstract

We introduce a method that accounts for errors caused by the slit function errors in an optimal estimation based spectral fitting process to improve ozone profile retrievals from the Ozone Monitoring Instrument (OMI) ultraviolet measurements (270-330 nm). Previously, a slit function was parameterized as a standard Gaussian by fitting the Full Width at Half Maximum (FWHM) of the slit function from climatological OMI solar irradiances. This cannot account for the temporal variation of slit function in irradiance, the intra-orbit slit function changes due to thermally-induced change and scene inhomogeneity, and potential differences in the slit functions of irradiance and radiance measurements. As a result, radiance simulation errors may be induced due to using the convolvinged reference spectra with incorrect slit functions. To better represent the shape of the slit functions, we implement a more generic super Gaussian slit function with two free parameters (slit width and shape factor); it becomes standard Gaussian when the shape factor is fixed to be 2. The effects of errors in slit function parameters on radiance spectra, referred as "Pseudo Absorbers (PAs)", are linearized by convolving high-resolution cross sections or simulated radiances with the partial derivatives of the slit function with respect to the slit parameters. The PAs are included in the spectral fitting scaled by fitting coefficients that are iteratively adjusted as elements of the state vector along with ozone and other fitting parameters. The fitting coefficients vary with cross-track and along-track pixels and show sensitivity to heterogeneous scenes. The total PA spectrum is quite similar in the Hartley band below 310 nm for both standard and super Gaussians, but is more distinctly structured in the Huggins band above 310 nm with the use of super Gaussian slit functions. Finally, we demonstrate that some spikes of fitting residuals are slightly smoothed by accounting for the slit function errors. Comparisons with ozonesondes demonstrate noticeable improvements with the use ofwhen using PAs for both standard and super Gaussians, especially for reducing the systematic biases in the tropics and mid-latitudes (mean biases of tropospheric column ozone reduced from -1.4 ~ 0.7 DU to 0.0 ~0.4 DU) and reducing the standard deviations of tropospheric ozone column differences at high-latitudes (by 1 DU for the super Gaussian). Comparisons with ozonesondes demonstrate that applying PAs eliminates the systematic biases in the tropics and mid-latitudes and thereby the mean biases of the tropospheric column ozone are reduced from -1.4 ~ 0.7 DU to 0.0 ~0.4 DU. In addition, the reduction of standard deviations is found in the high-latitude by 0.5 and 1.0 DU with standard and super Gaussians, respectively.Comparisons with ozonesondes demonstrate substantial improvements with the use of PAs for both standard and super Gaussians, especially for reducing the systematic biases in the tropics and mid-latitudes and reducing the standard deviations at

~~high-latitudes.~~ Including PAs also makes the retrievals consistent between standard and super Gaussians. This study corroborates the slit function differences between radiance and irradiance demonstrating that it is important to account for such differences in the ozone profile retrievals.

1. Introduction

The fitting of ~~the~~ measured spectra~~um~~ to ~~the~~ simulated spectra~~um~~ is the most basic concept for ~~the~~ analysis of the Earth's atmospheric constituents from satellite measurements. Therefore, ~~the~~ accurate calibration and simulation of measurements are essential for the successful retrieval of atmospheric constituents. The knowledge of the instrumental spectral response function (ISRF) or slit function could affect the accuracies of both calibration and simulation, as it is required for the convolution of a high-resolution reference spectrum ~~on~~to instrument's spectral resolution in the wavelength calibration and for the convolution of high-resolution absorption cross section spectra or simulated radiance spectra~~um~~ in the calculation of radiance at instrumental resolution. Compared to other trace gases, the retrieval of ozone profiles ~~could~~ can be more susceptible to the accuracy of ISRFs due to the large spectral range, where the radiance spans a few orders of magnitude and to the fact that the spectral fingerprint for the tropospheric ozone is primarily provided by the 3~~2~~10-330 nm absorption features residing in the temperature-dependent Huggins bands~~by narrow and weak absorption features of the temperature-dependent Huggins bands (320-360 nm)~~. Therefore, the efforts to~~of~~ characterize~~ing~~ and verify~~ing~~ the ISRFs have preceded the analyses of ozone profiles from ~~the~~ satellite and ~~/~~aircraft measurements (Liu et al., 2005, 2010; Cai et al., 2012; Liu et al., 2015; Sun et al. 2017; Bak et al., 2017).

For space-borne instruments, ISRFs are typically characterized as a function of the detector dimensions using a tunable laser source prior to the launch (Dirksen et al., 2006; Liu et al., 2015; van Hees et al., 2018) and directly used in ozone profile retrievals (e.g., Kroon et al., 2011; Mielonen et al., 2015; Fu et al., 2013; 2018). ~~.~~ However, the preflight measured ISRFs could be inconsistent with those after launch due to the orbital movement and the instrument temperature change (Beirle et al., 2017; Sun et al., 2017). Therefore, the post-launch ISRFs have been fitted from the preflight ones (e.g., Bak et al., 2017; Sun et al., 2017) or ~~been typically~~ parameterized through a cross-correlation of the measured solar irradiance to a high-resolution solar spectrum (Caspar and Chance, 1997), assuming Gaussian-like shapes (e.g., Liu et al. 2005; 2010). The direct retrieval of the ISRFs from radiances has not typically been done due to the complication of taking the atmospheric trace gas absorption and Ring effect into account in the cross-correlation procedure and the slow-down of the fitting process. However, slit function differences between radiance and irradiance could exist due to scene heterogeneity, differences in stray light between radiance and irradiance, and intra-orbit instrumental changes (such as ~~, and the~~ instrument temperature change) (Beirle et al., 2017; Sun et al., 2017). In addition, using temporally invariant slit functions derived from climatological solar spectra in the retrievals could cause the long-term trend errors if instrument degradation occurs. Therefore, there is room for improving our trace gas retrievals by accounting for the effects of the different ISRFs between radiance and irradiance on the spectral fitting ~~and~~ on ~~the~~ a pixel-to-pixel basis. The "Pseudo Absorber (PA)" is a common concept in spectral fitting to account for the effect of ~~the~~ physical phenomena that ~~is~~ are difficult or computationally demanding to be simulated in ~~the~~ radiative transfer calculations, like spectral misalignments (shift and stretch) between radiance and irradiance, Ring effect, spectral undersampling, and additive stray-light offsets. The pseudo absorption spectrum can be derived from a finite-different scheme (e.g. Azam and Richter, 2015) or a linearization scheme via a Taylor expansion (e.g. Beirle et al., 2013; 2017); the latter approach is more efficient than the former one, but less accurate because only the first term of the Taylor series is typically taken into account for simplicity. Beirle et al. (2013) introduced a linearization scheme to account for spectral misalignments between radiance and irradiance and then included them as a pseudo-absorber in DOAS-based NO_2 and BrO fittings. Similarly, Beirle et al. (2017) linearized the effect of the change of the ISRF parameterized as a super Gaussian on GOME-2 solar irradiance spectra to characterize the slit function change over time and wavelength. Sun et al. (2017) derived on-orbit slit functions from solar irradiance spectra measured by the Ozone Monitoring Instrument (OMI) (Levelt et al., 2006) assuming standard Gaussian, super Gaussian, and preflight ISRFs with adjusted widths. The derived on-orbit slit functions, showing significant cross-track dependence that cannot be represented by preflight ISRFs, substantially improve the retrievals by the Smithsonian Astrophysical Observatory (SAO) ozone profile algorithm. However, it is not fully understood why the use of super Gaussian or stretched preflight functions, which are supposed to better model the OMI spectra as indicated by smaller mean fitting residuals, does not improve the retrievals over the use of standard Gaussian especially in the standard deviations of the differences with relative to ozonesonde observations. This study suggests~~ed~~ that the slit functions derived from solar spectra might not fully represent those in radiance spectra.

As such, the objective of this paper is to ~~implement~~ expand the slit function linearization proposed by Beirle et al. (2017) into the optimal estimation based spectral fitting of the SAO ozone profile algorithm. The slit function linearization is used to account for the radiative transfer calculation errors caused by the slit functions differences between radiance and irradiance ~~We further improve the slit function parameterization by accounting for the differences between radiance and irradiance slit functions~~ on a pixel-by-pixel basis, and ultimately to improve OMI ozone profile retrievals. This paper is organized as follows: after a mathematical description of the linearization of slit function changes using the generic super Gaussian function, we introduce ~~how to apply~~ their~~m~~ practical application~~ly~~ in an optimal estimation based spectral fit procedure (Section 2). This linearization scheme is implemented differently ~~implemented~~, depending on the simulation scheme of measured spectra using high resolution ~~radiances~~ or effective cross section data, respectively. Section 3 characterizes the derived pseudo absorber spectra, along with ~~the~~ evaluations of ozone profile retrievals using independent ozonesonde observations as a reference dataset. Finally, the summary of this study is given in Section 4.

2. Method

2.1 Super Gaussian linearization

The slit function parameterization and linearization are briefly summarized ~~from~~ as in Beirle et al. (2017), focusing on what we need to derive the pseudo absorbers in the terms of the optimal estimation based fitting process. The slit function can be parameterized with the slit width w, and shape factor k assuming the supper Gaussian, S as:

$$S(\Delta\lambda) = A\,(w, k) \times exp\left[-\left|\frac{\Delta\lambda}{w}\right|^{k}\right], \qquad (1)$$

where $\mathrm{A}(w, k)$ is $\frac{k}{2\sigma_g \Gamma\left(\frac{1}{w}\right)}$ with Γ representing the gamma function. This equation allows many forms of distributions by varying k: the top-peaked function (k<2), the standard Gaussian function (k=2), and the flat-topped function (k>2). w is converted to the Full Width at Half Maximum (FWHM) via the relationship of $\mathrm{FWHM} = 2\sqrt[k]{ln2}\,w$. We investigate the impact of including one more slit parameter k on the OMI ISRF fitting results over the standard Gaussian using OMI daily solar measurements. As an example, time-series (2005-2015) of the fitted slit width and shape factor in 310-330 nm are displayed in Figure 1.a. The FWHM and shape factor of the super Gaussian function is on average 0.44 nm and 2.9, respectively, while the FWHM of the standard Gaussian is 0.395 nm. The sharp change and random-noise of these derived slit function parameters might be influenced by the decreasing signal-to-noise ratio (SNR) of solar spectra later in the OMI mission and radiometric errors in solar irradiance due to the row anomaly (Sun et al., 2017).~~The degradation of the OMI slit functions became relatively visible after 2011.~~ Figure 1.b illustrates t~~T~~he high wavelength stability (0.003 nm) ~~is seen in Figure 1b~~in the OMI mission, verifying that better calibration stability is performed with super Gaussian slit functions as abnormal deviations of wavelength shifts are derived with standard Gaussian slit functions.

The effect of changing the slit parameters p on the slit function can be linearized by the first-order Taylor expansion approximation around $\mathrm{S_o} = S(p_o)$:

$$\triangle \mathrm{S} = \mathrm{S} - \mathrm{S_o} \approx \triangle p \frac{\partial S}{\partial p}, \quad (2)$$

and thus the effect of changes of S on the convolved high-resolution spectrum can be parameterized as

$$\triangle \mathrm{I} = \mathrm{I} - \mathrm{I_o} \ = \mathrm{S} \otimes I_h - S_o \otimes I_h = \triangle \mathrm{S} \otimes I_h \ , (3)$$

where the convolved spectrum is I = S $\otimes I_h$. Consequently, the partial derivatives of I with respect to slit parameters~~,~~ *p* are defined as

$$\frac{\partial \mathrm{I}}{\partial p} = \frac{\partial \mathrm{S}}{\partial p} \otimes I_h \ . \ (4)$$

~~In~~ Beierle et al. (2017)~~, $\frac{\partial I}{\partial p}$~~ refers to $\frac{\partial \mathrm{I}}{\partial p}$ ~~J_p~~ as J_p~~,~~ "resolution correction spectra (RCS)". In Figure 2, we present an example of J_p over the typical ozone profile fitting range (270-330 nm) through the convolution of high-resolution ozone cross sections (δ_h) with the derivatives of the super Gaussian ($\frac{\partial S}{\partial p}$). The baseline $\mathrm{S_o}$ is defined with *w* =0.26 nm and *k*=2.6, which are averaged parameters from climatological OMI solar irradiance spectra in the UV2 band (310-330 nm). Note that this *w* value corresponds to a FWHM of 0.45 nm. The change of the assumed OMI slit function causes a highly structured spectral response over the whole fitting window. However, the relative magnitude of the responses with respect to both slit parameters is more distinct in the Huggins band (>310 nm) where narrow absorption features are observed as shown in Figure 2.a. An anti-correlation (-0.92) is found between $\frac{\partial \ln\delta}{\partial w}$ and $\frac{\partial \ln\delta}{\partial k}$ while the response of the unit change of the slit width to the convolved spectrum is dominant against that of the shape factor.

2.2 Implementation of the slit function linearization in the SAO ozone profile algorithm

In Beirle et al. (2017) a slit function linearization was implemented only to fit ~~a~~ solar irradiances from GOME~~-/~~2. We implement the slit function linearization to fit ~~a~~ radiances in the SAO ozone profile algorithm (Liu et al. 2010), which is routinely being performed to produce the OMI PROFOZ product (https://avdc.gsfc.nasa.gov/index.php?site=1389025893&id=74). Two spectral windows (~~i.e.,~~ 270-309 nm in the UV1 band and 312-330 nm in the UV2 band) are employed to retrieve ozone profiles from OMI BUV measurements. To match the different spatial resolutions between UV1 and UV2 bands, every two cross-track pixels are averaged for UV2 band, resulting into 30 positions with the spatial resolution of 48 km (across-track) × 13 km (along-track) at nadir position. Partial ozone columns at 24 layers between the surface and 60 km are iteratively estimated toward minimizing the fitting residuals between measured and simulated radiances and simultaneously between a priori and estimated ozone values using the ~~well-known~~ optimal estimation inversion method. ~~The non-linear optimal estimation based fitting is iterated~~

toward minimizing the fitting residuals between measured and simulated radiances and simultaneously between a priori and estimated ozone values. A priori ozone information is taken from a tropopause-based (TB) ozone profile climatology (Bak et al., 2013). The Vector Linearized Discrete Ordinate Radiative Transfer model (VLIDORT;) (Spurr, 2008) is used to simulate the radiances and their derivatives with respect to geophysical parameters. The radiance calculation is made for the Rayleigh atmosphere, where the incoming sunlight is simply absorbed by ozone and other trace gases, scattered by air molecules, and reflected by surfaces/clouds assumed as a Lambertian surface. Besides these, other physical phenomena, the others are treated as PAs to the spectral response such as Ring effect, additive offset, and spectral shifts due to misalignments of radiance relative to irradiance and ozone cross sections. In the SAO algorithm, these PAs are derived using the finite differences of the radiances with and without perturbation to a phenomenon, except for the Ring spectrum that is calculated using a first-order single scattering rotational Raman scattering model (Sioris and Evans, 2000).

In this paper, we introduce new PAs to account for the radiance simulation errors caused by the slit function errors. The OMI ISRFs have been parameterized as a standard Gaussian from climatological OMI solar irradiances for each UV1 and UV2 band and thereby these PAs could take into account the spectral fitting responses caused by temporal variations of the slit function. This ozone fitting procedure uses ISRFs to convolve high resolution absorption spectra, taken from Brion et al. (1993) for ozone absorption cross sections and Wilmouth et al. (1999) for BrO absorption cross sections. In DOAS analysis, the pseudo absorber is defined as $\frac{\partial S}{\partial p}\otimes\sigma_h$ (σ_h is a high-resolution absorption cross section), which could be calculated at a computationally low-cost. In theour optimal estimation based ozone profile retrievals, it is conceptually defined as $\frac{\partial S}{\partial p}\otimes I_h$ (I_h is a high-resolution simulated radiance), which is computationaly very expensive because of on-line radiative calculation for a ~ 60 nm wide fit window on the spatial pixel--to--pixel basis. We now introduce hereafter how to implement the slit function linearization to derive the derivatives of the OMI radiances with respect to to slit function changes in Our algorithm has implemented two different convolution processesradiative transfer calculationsapproaches used in the SAO ozone profile algorithm, ,i.e., the effective cross section approach in Liu et al (2010) and the updated high-resolution convolution approach described described in Kim et al. (2013), respectively. and thereby this paper also introduces how to derive the derivatives of the OMI radiances with respect to ISRF changes in these two approaches. Although the latter is the preferred approach in this study, we also implement and present the linearization with the first approach, which is typically used for other trace gas retrieval algorithms.

In Liu et al (2010), VLIDORT simulates the radiances at OMI spectral spect=--0ral grids (λ_{omi}) using effective cross sections that are produced by convolving high-resolution cross sections with the OMI

ISRFs. Therefore, we apply a similar convolution process of matching the high-resolution cross section spectra~~um~~ with OMI spectra~~um~~ to derive the partial derivative of σ_x with respect to slit parameter, p as follows:

$$\frac{\partial \sigma_x}{\partial p} = \frac{\partial S}{\partial p} \otimes \sigma_{x,h} \,, (5)$$

where $\sigma_{x,h}$ is a high-resolution absorption spectrum for ozone ~~and~~ or BrO~~, respectively~~. Due to the dominant ~~ozone~~ absorption of O_3 over ~~the~~ BrO ~~absorption~~, the derivative of the BrO cross section with respect to p is neglected here. This partial derivative of ozone is then converted to the partial derivative of radiance through the chain rule with the analytical ozone weighting function ($\frac{\mathrm{dlnI}}{\mathrm{dO_3}}$), calculated from VLIDORT, as follows:

$$\frac{\partial \mathrm{lnI}}{\partial p} = \frac{\partial ln\mathrm{I}}{\partial \mathrm{O_3}} \frac{\partial \sigma}{\partial p} \frac{O_3}{\sigma} \,. (6)$$

This simulation process is hereafter referred to as “effective resolution cross section (ER) simulation”.

As described in Kim et al. (2013), the radiative transfer calculation in the SAO ozone profile algorithm has been performed using high-resolution extinction spectra at the optimized sampling intervals for resolving the ozone absorption features, which are a ~1.0 nm below 300 nm and ~0.4 nm above 300 nm. These sampling intervals are coarser than actual OMI sampling grids with approximately half the number of wavelengths. The coarser sampled simulated radiances are then interpolated to a fine grid of 0.05 nm assisted by the weighting functions with respect to absorption and Rayleigh optical depth:

$$\mathrm{I}(\lambda_\mathrm{h}) = \mathrm{I}(\lambda_\mathrm{c}) + \frac{\partial \mathrm{I}\,(\lambda_\mathrm{c})}{\partial \Delta_l^{gas}} \left(\Delta_l^{gas}(\lambda_\mathrm{h}) - \Delta_l^{gas}(\lambda_\mathrm{c})\right) + \frac{\partial \mathrm{I}\,(\lambda_\mathrm{c})}{\partial \Delta_l^{ray}} \left(\Delta_l^{ray}(\lambda_\mathrm{h}) - \Delta_l^{ray}(\lambda_\mathrm{c})\right), (7)$$

where Δ_l^{gas} and Δ_l^{ray} are the optical thickness (the product of cross section and layer column density) at each layer for trace gas absorption and Rayleigh scattering, respectively. The convolution is then applied to these simulated high-resolution radiances, $\mathrm{I}(\lambda_\mathrm{h})$ with assumed slit functions and derivatives, respectively, and thereby $\mathrm{I}(\lambda_\mathrm{omi})$ and $\frac{\partial \mathrm{lnI}}{\partial p}$ is calculated. This simulation process is hereafter referred to as “high-resolution cross section (HR) simulation.”~~.~~ The ER simulation is more commonly implemented in ~~the~~ trace gas retrievals in the UV and visible, but the HR simulation allows for more accurate fitting residuals, to~~,~~ better than 0.1 % (Kim et al., 2013) as well as shorter computation time. $\frac{\partial \mathrm{lnI}}{\partial p}$ is scaled by the fitting coefficients, Δp, to account for the actual size of the spectral structures caused by the slit function differences between radiance and irradiance spectra. The ~~total~~ “pseudo absorber (PA)” for the s~~S~~uper Gaussian slit function linearization is expressed as:

$$PA = \partial \ln I = \frac{\partial \ln I}{\partial k}\,\Delta k + \frac{\partial \ln I}{\partial w}\,\Delta w. \quad (8)$$

In the form of the logarithm of normalized radiances, PA is physically related to the optical depth ~~change~~ change $\Delta\tau$. Figure 3 compares the partial derivatives of radiances to slit parameters, $\frac{dlnI}{dp}$ in HR and ER simulations. Little difference is found even though convolution error for ozone cross sections is only accounted for in the ER simulation due to the overwhelming impact of ozone cross section convolution errors over other cross section data. The amplitude of $\frac{dlnI}{dp}$ ~~PAs~~ varies with different satellite pixels (e.g., ozone profile shape, ~~angle~~ geometr~~ies~~y, and cloud/surface property), but the spectral peak positions do not change because ~~it~~ they arises from the errors due to the convolution ~~errors~~ process of high-resolution absorption cross-sections dominated by ozone~~ozone cross section~~. It should be noted that these spectral structures are weakly correlated with the partial derivatives of radiances with respect to other state vectors (ozone, BrO~~o~~, cloud fraction, surface albedo, radiance/irradiance shift, radiance/ozone cross section shift, Ring, ~~/~~mean fitting residual scaling factor) within ± 0.3 and ± 0.1 in the UV 1 and UV 2, respectively.

Furthermore, this linearization process can be formulated with n-order polynomial fitting parameters (Δp_i) to account for the wavelength-dependent change of the slit parameters around a central wavelength $\bar{\lambda}$, ~~and consequently, the total PA is~~which is expressed as

$$PA = \frac{\partial \ln I}{\partial k}\sum_{i=1}^{n}\Delta k_i \cdot \left(\lambda - \bar{\lambda}\right)^{n-1} + \frac{\partial \ln I}{\partial w}\sum_{i=1}^{n}\Delta w_i \cdot \left(\lambda - \bar{\lambda}\right)^{n-1}. \quad (9)$$

3. Results and Discussion

We characterize the effect of including the PA ($\frac{\partial \ln I}{\partial p} \cdot \triangle p$) on ozone profile retrievals using both Super Gaussian and standard Gaussian slit functions. Hereafter, the correction spectrum ($\frac{\partial \ln I}{\partial p}$) is derived using the HR simulation. The PA coefficient (Δp_i) (one for each channel and for each order) is included as part of the state vector to be iteratively and simultaneously retrieved with ozone. The a priori value is set to be zero for all fitting coefficients, while the a priori error is set to be 0.1, empirically. We should note that the empirical "soft calibration" is applied to OMI radiances before the spectral fitting, in order to eliminate the wavelength and cross-track dependent systematic biases, due to the interference of the PA coefficients with systematic measurement errors during the fitting process.

3.1 Characterization of the pseudo absorbers in ozone fitting procedure

Figure 4 displays how the zero-order PA coefficients (Δp) vary within one orbit when slit functions are assumed as standard and Super Gaussians, respectively, along with variation of cloud fraction, surface albedo, and cloud pressure from the retrievals. These ~~fitting coefficients~~retrieved coefficients physically represent the deviation of ISRFs in radiances from those in solar measurements. ~~difference of slit parameters between radiance and irradiance in this implementation. fitting.~~ We normalize them with the slit parameters derived from OMI solar irradiances for a better interpretation. Cross-track dependent features are shown in slit width. The relative change of the slit width is more distinct in the UV1 band than in the UV2 band, whereas the change of the shape factor is more distinct in the UV2 band. The UV2 slit widths increase typically within 5 % over the given spatial domain. However, the UV1 slit widths increase from 10 % at most pixels up to 50 % at off-nadir positions in the high latitudes, which might be caused by stray light differences between radiance and irradiance and intra-orbit instrumental changes. An abnormal change of the UV1 slit parameters due to the scene heterogeneity is detected at the along-track scan positions of ~300 and 900, respectively, where upper-level clouds are present. The UV2 shape factor changes show a coherent sensitivity to bright surfaces under clear-sky condition over the northern high latitudes. Fitting coefficients for the standard Gaussian show a quite similar spatial variation for the UV1 slit width (correlation = ~ 0.98), but an anti-correlation of ~ -0.62 for the UV2 slit width compared to those for Super Gaussian due to the interference between shape factor and slit width.

Examples of the ~~total~~ PAs (eq. 9) are illustrated in Figure 5 when (a) zero and (b) first-order polynomial coefficients are fitted, respectively. In t~~T~~he UV1 range, the sum of ~~total~~ PAs ~~spectrum~~multiplied by corresponding coefficients, regardless of which Gaussian is assumed as slit function, is very similar because the spectral structure caused by the slit width change is dominant. It implies that OMI ISRFs in the UV1 band are similar to the standard Gaussian, for both radiance and irradiance measurements, consistent with the pre-launch characterization (Dirksen et al., 2006). However, in the UV2 ~~band~~range, the spectral structures are generated by ~~PA is mostly contributed from~~ the shape factor change rather than the slit width change and therefore~~by~~ PAs show noticeable discrepancies for different Gaussian assumptions~~in the case of super Gaussian, and the total PA spectrum is more noticeable for super Gaussian.~~. Our results indicate that the PA for the shape factor change is required to adjust the spectral structures due to the differences in the slit functions between radiance and irradiance over the UV2 band. In the case of the wavelength dependent ~~ISRF~~ PA coefficient fit, the impact of first-order PAs on OMI radiances is relatively visible in the wavelength range of 300-310 nm. This result is physically consistent with the wavelength dependent property shown in the slit parameters derived from OMI irradiances as shown in Figure 6 where slit parameters are characterized in 10-pixel increments assuming the super Gaussian slit function. In UV1, the slit widths plotted as FWHM slightly decrease by ~ 0.1 nm at shorter wavelengths than 288 nm, but vary more sharply ~~vary~~ by up to ~ 0.2 nm at longer wavelengths. Compared to slit widths, the wavelength dependences of the shape factors are less noticeable, except at boundaries of the window. In the UV2 window, both slit width and shape factor are highly invariant.

3.2 Impact of including pseudo absorbers on ozone profile retrievals

Figures 7 to 9~~10~~ evaluate the impact of including zero-order PAs on ozone profile retrievals. Figure 7 illustrates how different assumptions in the slit functions affect the ozone profile retrievals with respect to the retrieval sensitivity and the fitting accuracy from the case shown in Figure 4. In this figure, the Degrees of Freedom for Signal (DFS) represents the independent pieces of ozone information available from measurements, which typically decreases as ozone retrievals are further constrained by other fitting variables. The reduced DFS values (< 5 %) imply that the ozone retrievals are correlated slightly with PAs. The fitting accuracy is assessed as the root mean square (RMS) of the relative differences (%) between measured and calculated radiances over the UV1 and UV2 ranges, respectively. Including the PAs makes little difference in the UV1 fitting residuals for most of individual pixels (1-5 %), but significantly reduces residuals in the UV2 range. The adjusted amounts of the residuals with PAs are generally larger when assuming super Gaussian slit functions. This comes from different assumptions for slit functions in deriving soft calibration spectra, where slit functions were parameterized as standard Gaussians. Therefore, applying soft calibration to OMI spectra entails somewhat artificial spectral structures if ISRFs are assumed as s~~S~~uper Gaussian in ozone retrievals, and hence the impact of PAs on the spectral fitting becomes more considerable. Figure 8 compares how the spectral residuals are adjusted with PAs when soft calibration is turned on and off, respectively. Using super Gaussians causes larger amplitudes of the spectral fitting residuals than using standard Gaussians, if soft calibration is turned on and PAs are excluded. On the other hand, some residuals are reduced and more broadly structured if soft calibration is turned off. Including PAs eliminates or ~~/~~reduces some spikes of fitting residuals as well as improves the consistency of the fitting accuracy between using standard and super Gaussians at wavelengths above 300 nm.

The benefit of this implementation on ozone retrievals is further assessed through comparison with Electrochemical Concentration Cell (ECC) ozonesondes collected from the WOUDC (https://woudc.org/) and SHADOZ (https://tropo.gsfc.nasa.gov/shadoz/) networks. This evaluation is limited to the period of 2005 through 2008 to avoid interferences with row-anomaly effects appearing in 2007 and becoming serious in early 2009 (Schenkeveld, et al 2017)~~ during the period 2005 to 2008~~. We select 13 SHADOZ sites in the tropics and 38 WOUDC sites in the northern mid/high latitudes. The collocation criteria is within +/- 1 ° in latitude and longitude and within 12 hours in time. For comparison, high-vertical resolution (~100 nm) profiles of ozonesondes are interpolated onto OMI retrieval grids (~2.5 km thick).

We limit OMI/ozonesonde comparisons to OMI solar zenith angle < 85°, effective cloud fraction < 0.4, surface albedo < 20 % (100 %) in tropics and mid-latitudes (high latitude), top altitude of ozonesondes > 30 km, ozonesonde correction factors ranging from 0.85 to 1.15 if they exist, and data gaps for each ozonesonde no greater than 3km. Comparisons between OMI and ozonesondes are performed for the tropospheric ozone columns (TCOs) over 3 different latitude bands and for ozone profiles including all the sites, with and without PAs (zero-order) for standard and super Gaussian slit function changes, respectively.

In Table 1, ~~Figure 9 shows~~ the comparison statistics ~~s~~ of tropospheric ozone columns between OMI and ozonesonde are summarized as ~~scatter plots~~a function of latitude bands. Without using PAs, the comparison results show a noticeable discrepancy in mean biases (1.3-2.1 DU or 3.9-6.4%) due to different assumptions on the slit function shape, with ~~Without using PAs, the retrievals show significant differences of (1.2-2.2 DU or 3.8-6.4%) especially in mean biases between super and standard Gaussians, with negative~~ positive biases of 0.~~2~~3-0.7 DU for super Gaussians and ~~positive~~ negative biases of ~~0~~1.~~8~~0-1.~~5~~ 4 DU for standard Gaussians. Overall, OMI retrievals are in a better agreement with ozonesonde measurements using super Gaussians. The correlations and standard deviations are very similar in the tropics and mid-latitudes, but the retrievals with standard Gaussians show better correlation and smaller standard deviations ~~in~~ at high-latitudes. ~~Consistent with Sun~~As in Sun et al. (2017), the retrievals show significant differences between using standard and super Gaussians, although there are some inconsistencies in comparing OMI and ozonesondes; the main inconsistent factors are~~ listed as following~~: In this study, soft calibration is turned on and a priori information is taken from the TB climatology to perform OMI ozone profile retrievals, whereas soft calibration is turned off and a priori information is taken from the LLM climatology in Sun et al. (2017). OMI/ozonesonde data filtering criteria are quite similar to each other, except that the criteria of the solar zenith angle and cloud fraction are relaxed from 75° and 0.3 to 85° and 0.4, respectively, and the adjustment of ozonesondes with correction factors given for the WOUDC dataset is turned on in this study. Comparison is performed by latitudes here whereas global comparison is analyzed in Sun et al. (2017). After accounting for the slit differences between radiances and irradiances using PAs, the retrievals are ~~significantly~~ improved for both standard and super Gaussians and these two retrievals become consistent except for the use of super Gaussians in the tropics. The mean biases in the tropics and mid-latitudes are almost eliminated, ~~to within 0.3 DU,~~ but the standard deviations and correlation do not change much~~, slightly worse in the tropics and better in the mid-latitudes~~. In the high-latitudes, the standard deviations and correlation are significantly improved due to applying PAs ~~when~~with super Gaussians ~~are assumed to be~~ ISRFs. ~~especially for using super Gaussians,~~

~~but the mean biases are similar to the standard Gaussian without PAs.~~ The lack of improvement with PAs in the tropics with super Gaussians illustrates that ISRFs of radiances are quite similar to those of irradiances in the tropics, while super Gaussians better parameterize OMI ISRFs than standard Gaussians. This is consistent with the comparison of the fitting accuracy of the UV2 band as shown in Figure 7, where the fitting residuals are slightly reduced in the tropics when super Gaussians are linearized, but the standard Gaussian linearization significantly improves the fitting accuracy. The mean biases of the profile comparison as shown in Figure ~~10~~ 9 clearly show~~s~~ that including PAs to account for ISRF differences ~~significantly~~ reduces mean biases ~~of~~by up to ~ 5 % below 10 km ~~below 10 km~~ and their general altitude dependence, and improves the consistency between using standard and super Gaussians; in addition, the standard deviations are slightly improved ~~also show noticeable improvement~~ in the 10-20 km altitude range~~ of 10-20 km~~ for both Gaussians. The ~~significant~~ improvement at all latitudes corroborates the change of ISRFs between radiance and irradiance along the orbit as conjectured by Sun et al. (2017). The consistency between using standard and super Gaussians after using PAs is mainly because there is strong anti-correlation between the slit width and shape partial derivatives as shown in Figure 2, so the adjustment of slit width only in the use of standard Gaussians can achieve almost the same effect as the adjustment of both parameters in the use of super Gaussians. Accounting for the wavelength dependent change of the ISRFs with first-order PAs makes insignificant differences to both fit residuals and ozone retrievals (not shown here). This could be mainly explained ~~with~~ by the fact of ~~the~~ negligible wavelength dependence of OMI ISRFs especially in UV2 as shown in Figure 5, where the PA spectrum $(\frac{\partial \ln I}{\partial p} \cdot \Delta p)$ shows almost no variance~~,~~ except at the upper boundary of ~~the~~ UV1, as well as in Figure 6 where the UV2 slit parameters derived from irradiances in the sub-fit windows vary within 0.05 nm for FWHM and 0.2 for shape factor.

4. Summary

The knowledge of the Instrument Spectral Response Functions (ISRFs) or slit functions is important for ozone profile retrievals from the Hartley and Huggins bands. ISRFs can be measured in the laboratory prior to launch, but they have been typically derived from solar irradiance measurements assuming Gaussian-like functions in order to account for the effect of the ISRF changes after launch. However, the parameterization of the ISRFs from solar irradiances could be inadequate for achieving a high accuracy of the fitting residuals as ISRFs in radiances could significantly deviate from those in solar radiances (Beirle et al., 2017) and might affect ozone profile retrievals as suggested in Sun et al. (2017). Therefore, this study implements a linearization scheme to account for the spectral errors caused by the ISRF~~s~~ changes as Pseudo Absorbers (PAs) in an optimal estimation based fitting procedure for retrieving ozone profiles from OMI BUV measurements using the SAO ozone profile algorithm. The ISRFs are assumed to be the generic super Gaussian that can be used as standard Gaussian when fixing the shape factor to 2. This linearization was originally introduced in Beirle et al. (2017) for DOAS analysis, but this study extends this application and more detail how to implement in practice using two different approaches to derive radiance errors from slit function partial derivatives with respect to slit parameters. These two approaches correspond to the two methods of simulating radiances at instrument spectral resolution, one using effective cross sections which were previously used in the SAO ozone profile algorithm and are still used in most of the trace gas retrievals from the UV and visible, and the other calculating radiances at high resolution before convolution, which is the preferred method in the SAO ozone profile algorithm. Consistent PAs are derived with these two approaches, as expected.

The fitting coefficients ($\triangle p$) to the PAs, representing the difference of slit parameters between radiance and irradiance, are iteratively fitted as part of the state vector along with ozone and other parameters. The UV1 slit parameters show distinct cross-track-dependent differences, especially in high -latitudes. In addition, an abnormal $\triangle$ p caused by scene heterogeneity is observed around bright surfaces and cloudy scenes. The ~~total~~ PA spectrum ($\frac{\partial I}{\partial p} \cdot \triangle p$) illustrates that the slit width change causes most of the spectral structures in the UV1 band because the OMI ISRFs are close to Gaussian. Otherwise, the ISRF change results into different spectral responses in the UV2 band with different Gaussian functions because the adjustment of the shape factor becomes more important in accounting for the convolution error when using super Gaussians.

Insignificant wavelength dependence on OMI slit functions is demonstrated from slit function parameters derived from irradiances in the sub-fit window, which leads to little difference in ozone profile retrievals when zero and first-order wavelength dependent PA coefficients are implemented to fit the spectral structures caused by slit function errors, respectively. Therefore we evaluate the benefit of including the zero-order PAs fit on both the accuracy of the fitting residuals and the quality of retrieved ozone profiles through validation against ozonesonde observations. Some spikes in the fitting residuals are reduced or eliminated. Commonly, including PAs makes little change on both fit residuals and ozone retrievals in the tropics if ~~a~~ super Gaussians are assumed as ISRFs but this is not the case for the standard

Gaussian assumption. In the TCO comparison between OMI and ozonesonde, the mean biases are reduced by 0.2 (0.6) DU and 0.6 (1.4) DU in the tropics (mid-latitude) when super and standard Gaussians are linearized, respectively. In particular, applying PA improves the standard deviations ~~in in~~at high latitudes by 1.0 DU for super Gaussian and 0.5 DU for standard Gaussian. ~~Retrievals using standard and super Gaussians agree better if slit function errors are accounted for by including PAs. Using PAs ultimately demonstrates substantial improvement of ozone profile retrievals in the comparison of~~

~~tropospheric ozone columns and ozone profiles up to 30 km. Using super Gaussians, the TCO comparison shows significant improvement in mean biases in mid-latitudes and in standard deviations in high-latitudes. Using standard Gaussians, the TCO comparison also shows significant improvement in mean biases in the tropics. Using PAs ultimately demonstrates substantial improvement of ozone profile retrievals in the comparison of tropospheric ozone columns and ozone profiles up to 30 km.~~ The profile comparison generally shows improvements in mean biases (~ 5% in the lower troposphere) as well as in standard deviation, ~~in~~slightly in the altitude range 10-20 km by applying PAs. More importantly, using these PAs make the retrieval consistent between standard and super Gaussians. Such consistency is due to the anti-correlation between slit width and shape PAs. This study demonstrates the slit function differences between radiance and irradiance and their~~its~~ usefulness to account for such differences on ~~the~~ a pixel-to-pixel basis. In this experiment, the soft spectrum, derived with the standard Gaussian assumption, is applied to remove systematic measurement errors before spectral fitting, indicating that the evaluation of ozone retrievals might be unfairly performed for the super Gaussian function implementation. Nonetheless, OMI ozone profile retrievals show better agreement with ozonesonde observations when the super Gaussian is linearized. Actually, the fitting residuals are slightly more broadly structured with super Gaussians than with standard Gaussians if the soft-calibration and PAs are turned off, indicating the benefit of deriving a soft calibration with the super Gaussians. Therefore, there is still room for achieving better benefits when using the PAs on ozone profile retrievals by applying the soft calibration derived with super Gaussians.

Acknowledgements

We acknowledge the OMI science team for providing their satellite data and the WOUDC and SHADOZ networks for their ozonesonde datasets. Research at the Smithsonian Astrophysical Observatory by J. Bak, X. Liu, K. Sun, and K. Chance was funded by NASA Aura science team program (NNX14AF16G & NNX17AI82G). Research at Pusan National University by J. H Kim was ~~also~~ supported by the Korea Ministry of Environment (MOE) as the Public Technology Program based on Environmental Policy (2017000160001).

References

Azam, F. and Richter, A.: GOME2 on MetOp: Follow on analysis of GOME2 in orbit degradation, Final report, EUM/CO/09/4600000696/RM, 2015, available at: http://www.doas bremen.de/reports/gome2_degradation_follow_up_final_report.pdf (last access: 7 September 2016), 2015.

Bak, J., Liu, X., Wei, J. C., Pan, L. L., Chance, K., and Kim, J. H.: Improvement of OMI ozone profile retrievals in the upper troposphere and lower stratosphere by the use of a tropopause-based ozone profile climatology, Atmos. Meas. Tech., 6, 2239–2254, doi:10.5194/amt-6-2239-2013, 2013.

Bak, J., Liu, X., Kim, J.-H., Haffner, D. P., Chance, K., Yang, K., and Sun, K.: Characterization and correction of OMPS nadir mapper measurements for ozone profile retrievals, Atmos. Meas. Tech., 10, 4373-4388, https://doi.org/10.5194/amt-10-4373-2017, 2017.

Beirle, S., Sihler, H., and Wagner, T.: Linearisation of the effects of spectral shift and stretch in DOAS analysis, Atmos. Meas. Tech., 6, 661–675, doi:10.5194/amt-6-661-2013, 2013.

Beirle, S., Lampel, J., Lerot, C., Sihler, H., and Wagner, T.: Parameterizing the instrumental spectral response function and its changes by a super-Gaussian and its derivatives, Atmos. Meas. Tech., 10, 581-598, https://doi.org/10.5194/amt-10-581-2017, 2017.

Brion, J., Chakir, A., D. Daumont, D., and Malicet, J.: High-resolution laboratory absorption cross section of O3. Temperature effect, Chem. Phys. Lett., 213(5–6), 610– 612, 1993.

Cai, Z., Liu, Y., Liu, X., Chance, K., Nowlan, C. R., Lang, R., Munro, R., and Suleiman, R.: , Characterization and correction of Global Ozone Monitoring Experiment 2 ultraviolet measurements and application to ozone profile retrievals, J. Geophys. Res., 117, D07305, doi:10.1029/2011JD017096, 2012.

Caspar, C. and Chance, K.: GOME wavelength calibration using solar and atmospheric spectra, Third ERS Symposium on Space at the Service of our Environment, Florence, Italy, 14–21 March, 1997.

Dobber, M., Voors, R., Dirksen, R., Kleipool, Q., and Levelt, P.: The high-resolution solar reference spectrum between 250 and 550 nm and its application to measurements with the Ozone Monitoring Instrument, Solar Physics, 249, 281–291, 2008.Kim, P. S., Jacob, D. J., Liu, X., Warner, J. X., Yang, K., Chance, K., Thouret, V., and Nedelec, P.: Global ozone–CO correlations from OMI and AIRS: constraints on tropospheric ozone sources, Atmos. Chem. Phys., 13, 9321-9335, https://doi.org/10.5194/acp-13-9321-2013, 2013.

Fu, D., Worden, J. R., Liu, X., Kulawik, S. S., Bowman, K. W., and Natraj, V.: Characterization of ozone profiles derived from Aura TES and OMI radiances, Atmos. Chem. Phys., 13, 3445-3462, https://doi.org/10.5194/acp-13-3445-2013, 2013.

Kim, P. S., Jacob, D. J., Liu, X., Warner, J. X., Yang, K., Chance, K., Thouret, V., and Nedelec, P.: Global ozone–CO correlations from OMI and AIRS: constraints on tropospheric ozone sources, Atmos. Chem. Phys., 13, 9321-9335, https://doi.org/10.5194/acp-13-9321-2013, 2013.

Fu, D., Kulawik, S. S., Miyazaki, K., Bowman, K. W., Worden, J. R., Eldering, A., Livesey, N. J., Teixeira, J., Irion, F. W., Herman, R. L., Osterman, G. B., Liu, X., Levelt, P. F., Thompson, A. M., and Luo, M.: Retrievals of tropospheric ozone profiles from the synergism of AIRS and OMI: methodology and validation, Atmos. Meas. Tech., 11, 5587-5605, https://doi.org/10.5194/amt-11-5587-2018, 2018.

Kroon, M., de Haan, J. F., Veefkind, J. P., Froidevaux, L., Wang,R., Kivi, R., and Hakkarainen, J. J.: Validation of operational ozone profiles from the Ozone Monitoring Instrument, J. Geo-phys. Res., 116, D18305, doi:10.1029/2010JD015100, 2011.

Levelt, P. F., van den Oord, G. H. J., Dobber, M. R., Malkki, A., Visser, H., de Vries, J., Stammes, P., Lundell, J. O. V., and Saari, H.: The ozone monitoring instrument, IEEE Transactions on Geoscience and Remote Sensing, 44, 1093–1101, doi:10.1109/TGRS.2006.872333, 2006.

Liu, X., Chance, K., Sioris, C. E., Spurr, R. J. D., Kurosu, T. P., Martin, R. V., and Newchurch, M. J.: Ozone profile and tropospheric ozone retrievals from Global Ozone Monitoring Experiment: algorithm description and validation, J. Geophys. Res., 110, D20307, doi: 10.1029/2005JD006240, 2005.

Liu, X., Bhartia, P.K, Chance, K, Spurr, R.J.D., and Kurosu, T.P.: Ozone profile retrievals from the ozone monitoring instrument. Atmos. Chem. Phys., 10, 2521–2537, 2010.

Liu, C., Liu, X., Kowalewski, M.G., Janz, S.J., González Abad, G., Pickering, K.E., Chance, K., and Lamsal., L.N.: Characterization and verification of ACAM slit functions for trace gas retrievals during the 2011 DISCOVER-AQ flight campaign, Atmos. Meas. Tech., 8, 751-759, doi:10.5194/amt-8-751-2015, 2015.

Mielonen, T., de Haan, J. F., van Peet, J. C. A., Eremenko, M., and Veefkind, J. P.: Towards the retrieval of tropospheric ozone with the Ozone Monitoring Instrument (OMI), Atmos. Meas. Tech., 8, 671-687, https://doi.org/10.5194/amt-8-671-2015, 2015.

Schenkeveld, V. M. E., Jaross, G., Marchenko, S., Haffner, D., Kleipool, Q. L., Rozemeijer, N. C., Veefkind, J. P., and Levelt, P. F.: In-flight performance of the Ozone Monitoring Instrument, Atmos. Meas. Tech., 10, 1957-1986, https://doi.org/10.5194/amt-10-1957-2017, 2017.

Sioris, C. E. and Evans, W. F. J.: Impact of rotational Raman scattering in the O_2 A band, Geophys. Res. Lett., 27, 4085–4088, 2000.

Spurr, R. J. D.: Linearized pseudo-spherical scalar and vector discrete ordinate radiative transfer models for use in remote sensing retrieval problems, in: Light Scattering Reviews, edited by: Kokhanovsky, A., Springer, New York, 2008.

Sun, K., Liu, X., Huang, G., González Abad, G., Cai, Z., Chance, K., and Yang, K.: Deriving the slit functions from OMI solar observations and its implications for ozone-profile retrieval, Atmos. Meas. Tech., 10, 3677-3695, https://doi.org/10.5194/amt-10-3677-2017, 2017.

van Hees, R. M., Tol, P. J. J., Cadot, S., Krijger, M., Persijn, S. T., van Kempen, T. A., Snel, R., Aben, I., and Hoogeveen, Ruud W. M.: Determination of the TROPOMI-SWIR instrument spectral response function, Atmos. Meas. Tech., 11, 3917-3933, https://doi.org/10.5194/amt-11-3917-2018, 2018.

Wilmouth, D. M., Hanisco, T. F., Donahue, N. M., and Anderson, J. G.: Fourier transform ultraviolet spectroscopy of the $A^2\Pi_{3/2} - X^2\Pi_{3/2}$ Transition of BrO, J. Phys. Chem. A., 103(45), 8935– 8945, 1999.

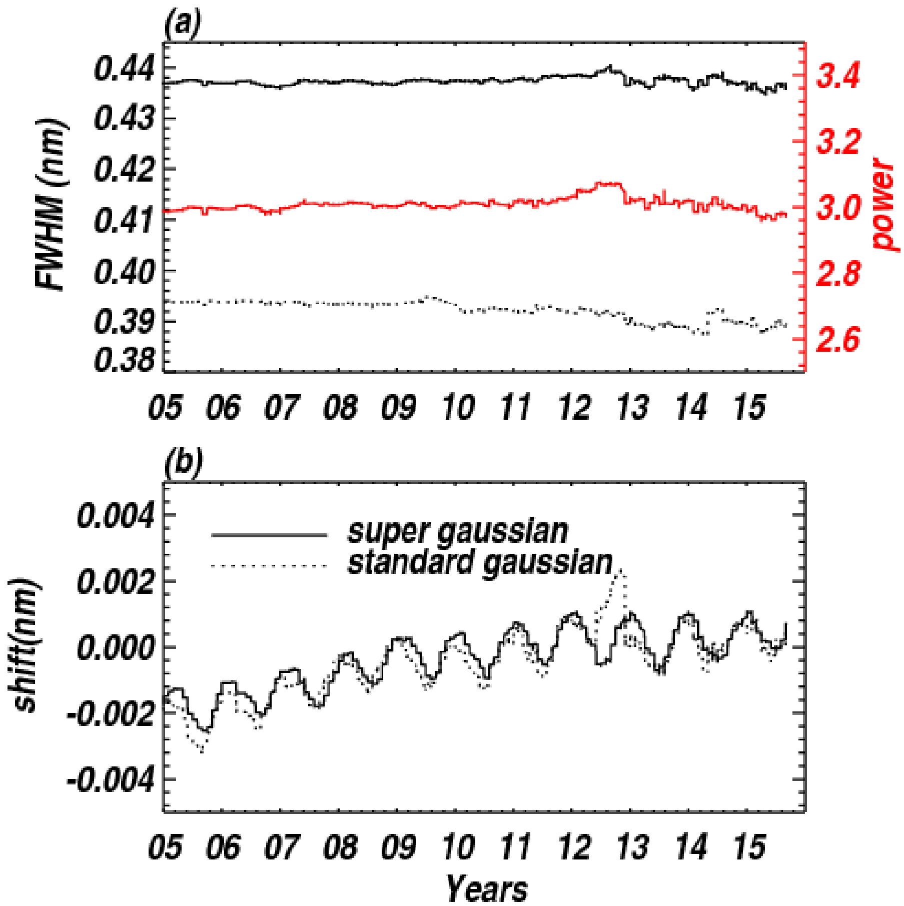

Figure 2~~1~~. Time series of (a) slit parameters and (b) wavelength shifts for OMI daily irradiance measurements (310-330 nm) at nadir cross track position when s~~S~~uper Gaussians (solid line) and standard Gaussians (dotted line) are parameterized as slit function shapes, respectively.

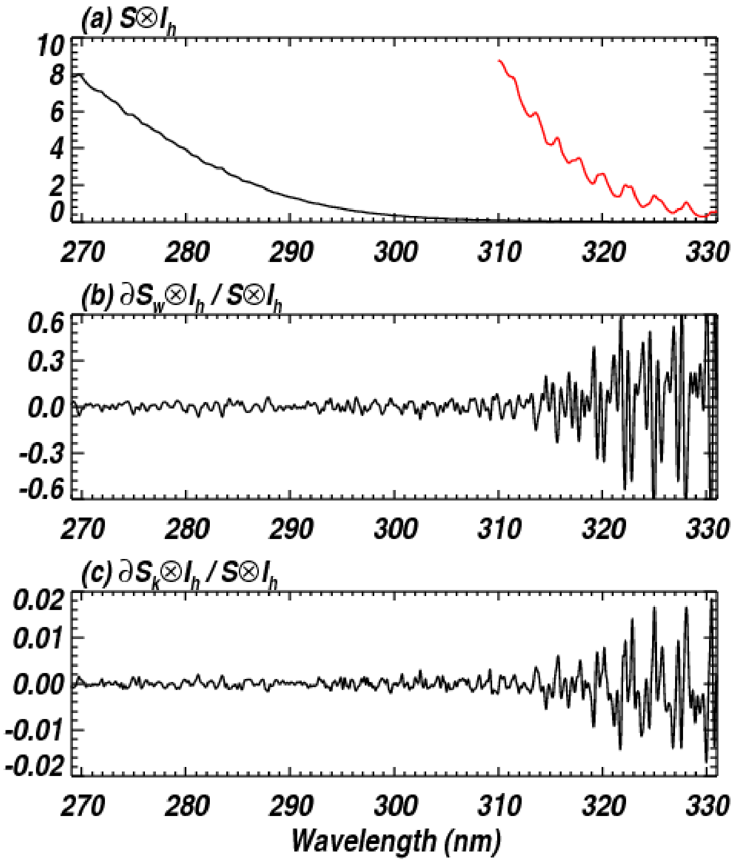

Figure 2. (a) Ozone absorption cross sections (cm^2/molecule) (δ_h) at different scales (red and black) at a representative temperature (238.12 K) calculated via convolution of high-resolution (0.01 nm) reference spectrum with the sSuper Gaussian slit function, S ($k = 2.6, \mathrm{w} = 0.26$ nm). (b) and (c) its derivatives with respect to slit parameters ($\partial S_p = \frac{\partial S}{\partial p}$), w and k, respectively, normalized to the convolved cross sections.

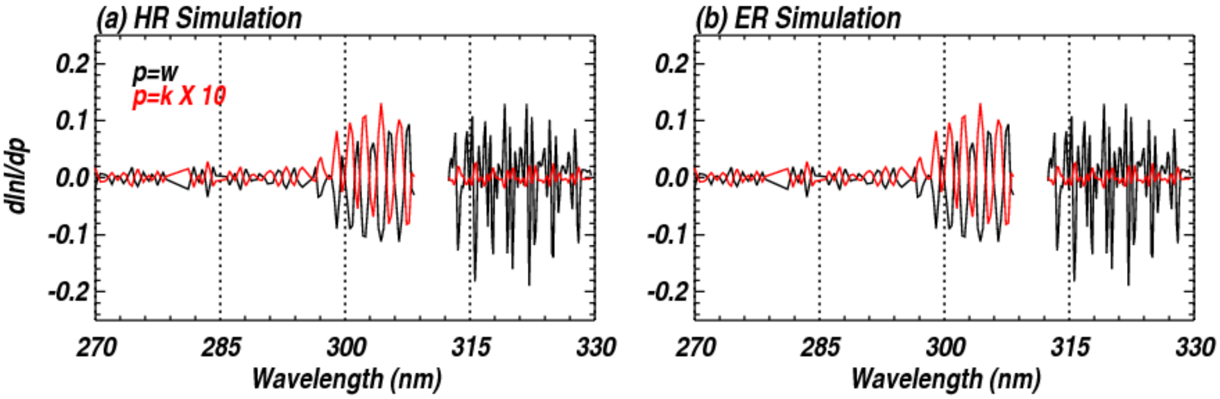

Figure 3. Derivatives of an OMI radiance spectrum simulated using high-resolution (HR) and effective resolution (ER) cross section spectra with respect to slit parameters assuming a s~~S~~uper Gaussian function. $\mathrm{dlnI}/\mathrm{d}k$ is multiplied by a factor of 10 to visually match $\mathrm{dlnI}/\mathrm{d}w$ ~~in~~ on the same y-axis.

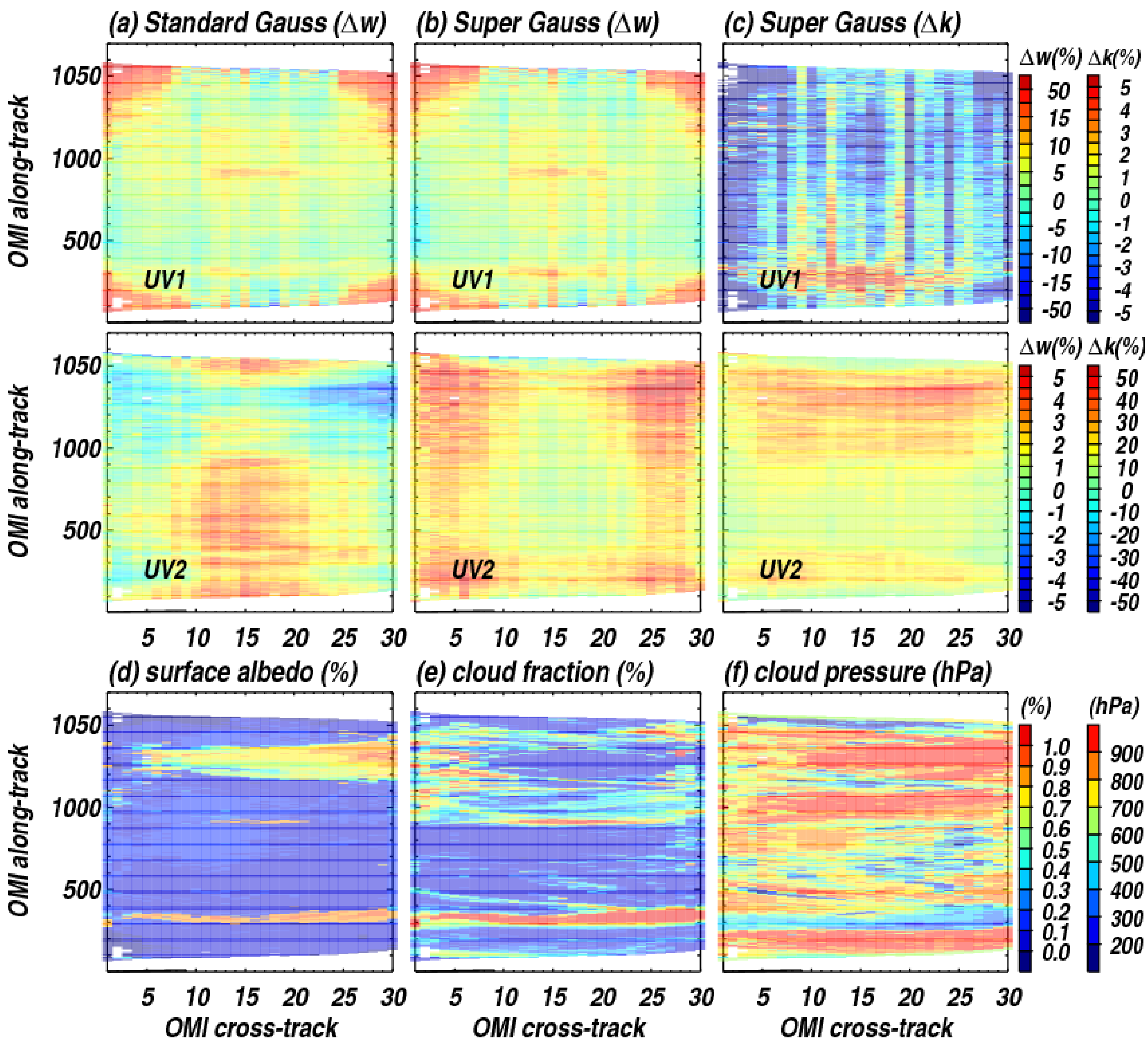

Figure 4. Pseudo absorption coefficients ($\Delta w, \Delta k$) for fitting ~~the~~ OMI radiances ~~due~~ to account for slit function changes assuming (a) standard Gaussian and (b-c) s~~S~~uper Gaussian, ~~within~~ for the first orbit of measurements on 1 July 2006, with (d-f) the corresponding geophysical parameters. Δw and Δk ~~is~~ are displayed after being normalized with w_o, and k_o, the slit parameters derived from OMI solar irradiance measurements.

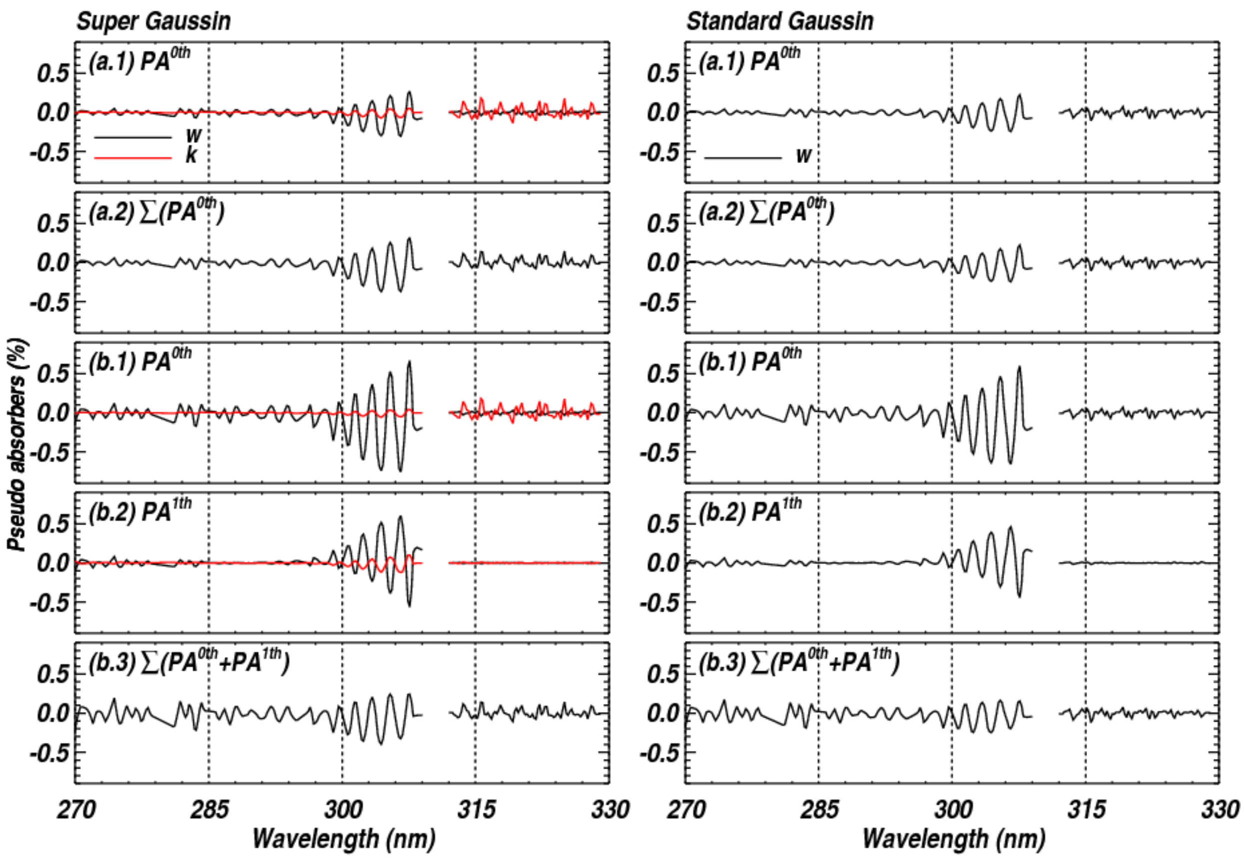

Figure 5. (a.1) Pseudo absorber spectra multiplied by corresponding zero order coefficients, ($\frac{\partial lnI}{\partial p} \times \Delta p_o$) and (a.2) the sum of them for zero order slit parameters for (left) sSuper Gaussian and (right) sStandard Gaussian function parameterizations, respectively. and (a.2) its total spectra for (left) Super Gaussian and (right) Standard Gaussian function parameterizations, respectively. **(b)** is s**Same as (a), but for first order polynomial** coefficients, $\frac{\partial lnI}{\partial p} \times \Delta p_i \left(\lambda - \bar{\lambda}\right)^i (i = 0,1)$ fit**. Th**ise case example **represents an average at nadir in the latitude zone 30°-60°N** from measurements used in Figure 4..

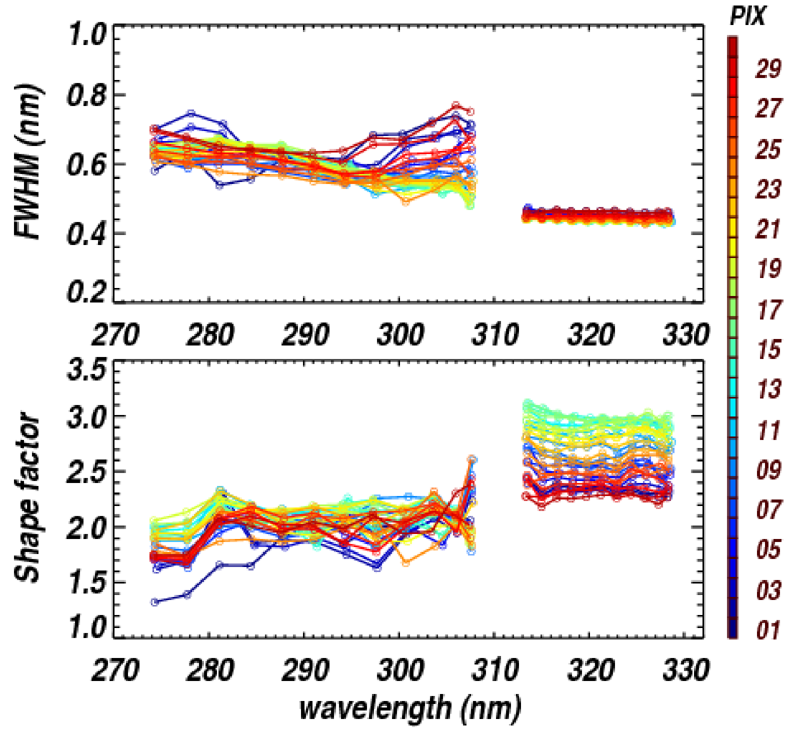

Figure 6. OMI ISRF FWHM (nm) and shape factor (k) as functions of the center wavelength, as derived from OMI solar irradiances assuming Super Gaussian functions over a range of 31 spectral pixels in 10-pixel increments. Different colors represent different cross-track positions from 1 (blue) to 30 (red).

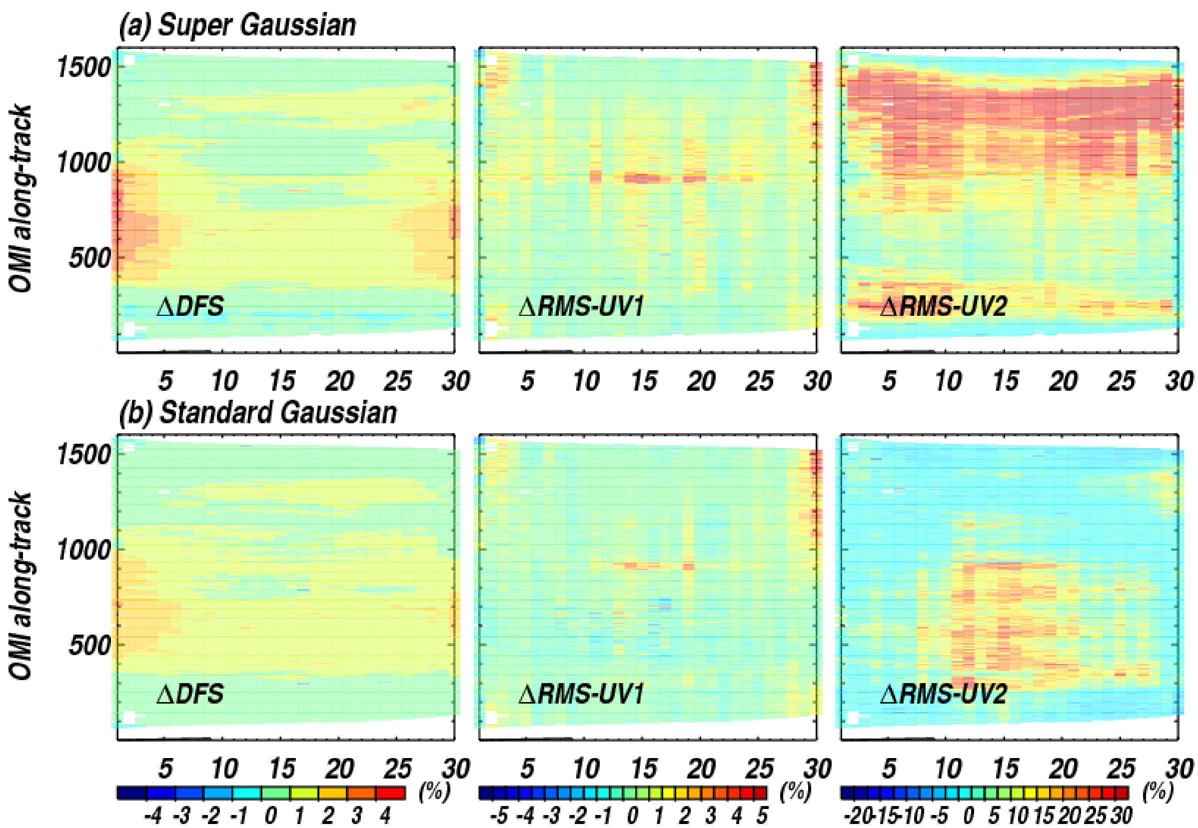

Figure 7. Same as Figure 4, but for comparisons of the Degrees of Freedom for Signal (DFS) and the Root Mean Square (RMS) of spectral fitting residuals in UV 1 and UV2 with and without zero-order pseudo absorber. Positive values indicate that both fitting residuals and DFSs are reduced due to the pseudo absorber.

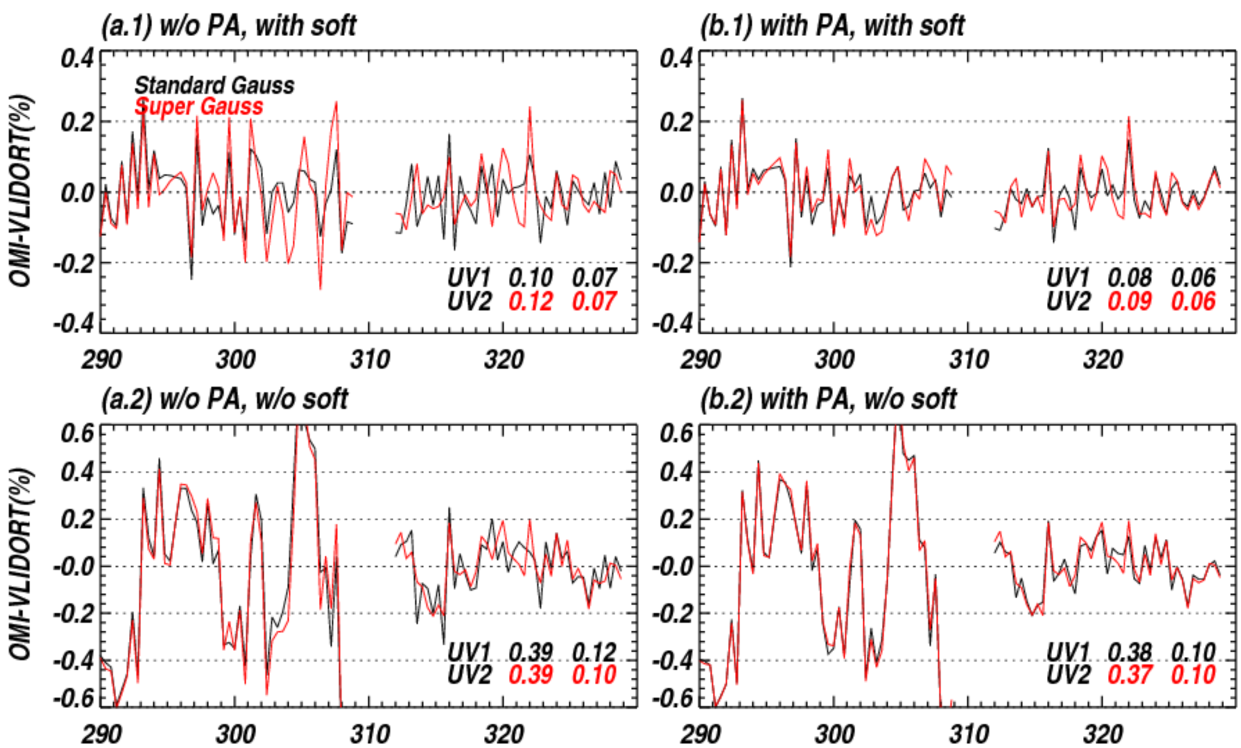

Figure 8. Average differences (%) between measured (OMI) and simulated (VLIDORT) radiances ~~(residuals)~~ at the nadir cross-track pixel in the tropics (30°S-30°S) from measurements used in Figure 4, without (a) and with (b) zero-order pseudo absorbers (PA) when the standard Gaussian (black line) and the s~~S~~uper Gaussian (red line) are assumed as ISRFs, respectively. Upper/lower panels represent the fitting results with soft calibration being turned on/off. The residuals in the UV1 (< 310 nm) are scaled by a factor of 2 to fit in the given y-axis. In the legend, the RMS of residuals (%) are given for UV1 and UV2 wavelength ranges, respectively.

Table 1. Comparison Statistics (Mean Bias in DU/%, 1σ Standard Deviation in DU/%, the Pearson Correlation Coefficient, number of collocations) of OMI and ozonesonde tropospheric column ozone from 2005 to 2008 over (a) tropical, (b) midlatitude, and (c) high-latitude stations.

(a) Tropics (30°S-30°N)			
Super Gaussian		Standard Gaussian	
With PA	w/o PA	With PA	w/o PA
-0.1±5.1DU (-0.3+15.8%) R=8.2, N=580	0.3±4.9DU (0.8±15.5%) R=0.83, N= 580	-0.4±5.3DU (-1.2±16.3%) R=0.81, N=582	-1.0±5.1DU (-3.1±16.0%) R=0.83, N=579
(b) Midlatitude (30°N-60°N)			
Super Gaussian		Standard Gaussian	
With PA	w/o PA	With PA	w/o PA
-0.1±4.9DU (0.0±14.5%) R=0.83, N=2336	0.7±5.0DU (2.3±15.0%) R=0.82, N=2333	0.0±5.0DU (0.3±15.0%) R=0.82, N=2315	-1.4±4.9DU (-4.1±14.6%) R=0.83, N=2317
(c) High-latitude (60°N-90°N)			
Super Gaussian		Standard Gaussian	
With PA	w/o PA	With PA	w/o PA
-0.7±5.2DU (-2.1±18.4%) R=0.61, N=447	0.3±6.2DU (1.5±22.2%) R=0.53, N=448	-0.6±4.9DU (-1.7±17.1%) R=0.65, N=433	-1.0±5.4DU (-3.2±18.7%) R=0.60, N=433

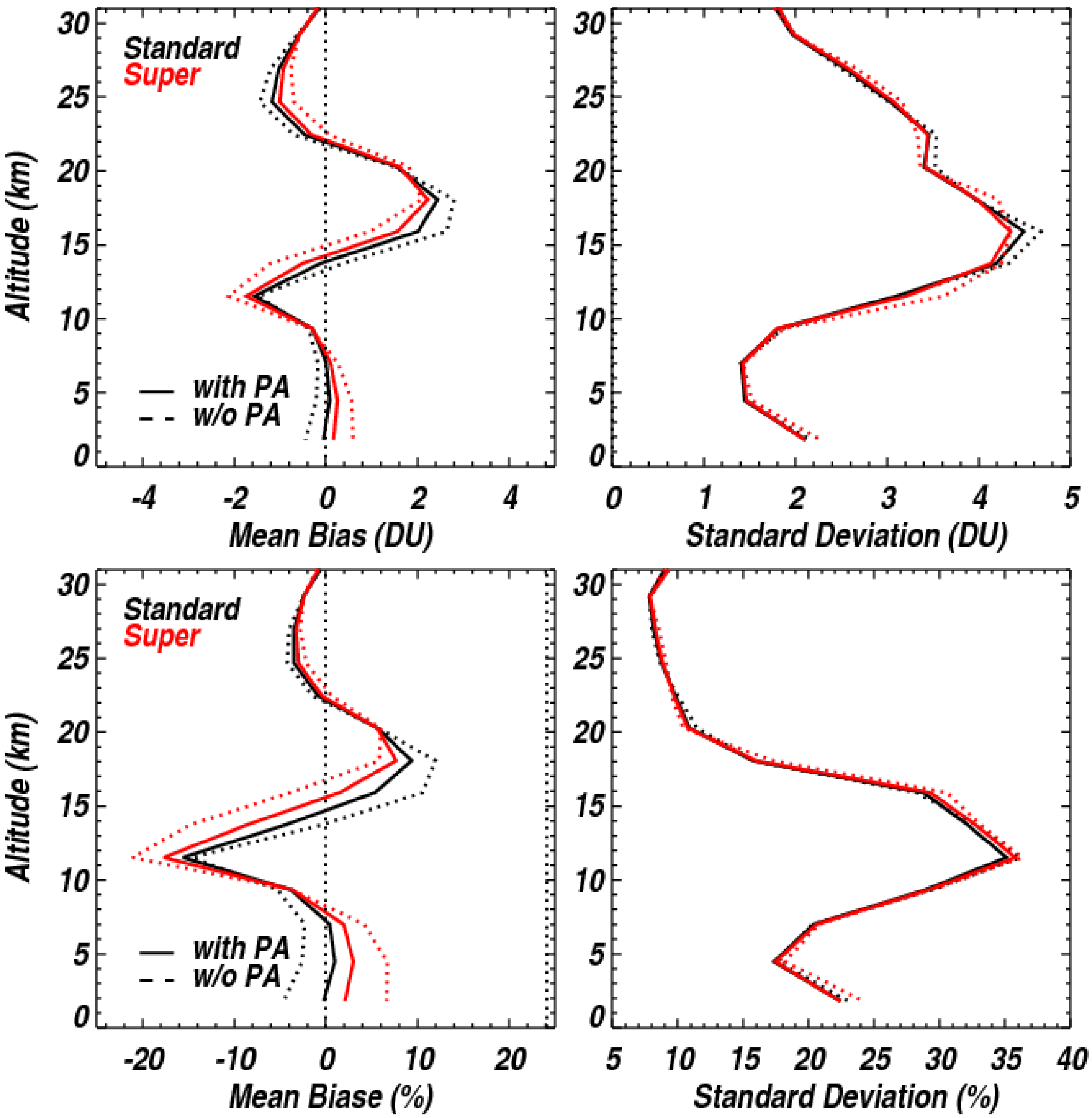

Figure 9~~10~~. Same as Table 1, but for ~~–g~~Global mean biases ~~at each OMI layer~~ and 1 σ standard deviations of the differences between OMI and ozonesondes at each OMI layer, with different slit function assumptions/implementations. The absolute and relative differences are used in the upper and lower ~~comprisons~~comparisons, respectively.